

Cite this: *New J. Chem.*, 2011, **35**, 1809–1816

www.rsc.org/njc

PAPER

Site-specific immobilization of cytochrome c on mesoporous silica through metal affinity adsorption to enhance activity and stability

Shih-Hsun Cheng,^a Kun-Che Kao,^b Wei-Neng Liao,^a Li-Ming Chen,^a Chung-Yuan Mou^b and Chia-Hung Lee^{*a}

Received (in Montpellier, France) 19th March 2011, Accepted 1st June 2011

DOI: 10.1039/c1nj20255c

We report a hydrothermally stable and highly reactive cytochrome c (cyt c) immobilized in the nanochannels of mesoporous silica (SBA-15) through a metal affinity interaction. Due to the strong affinity of mercury–sulfuric bonds, we modified the SBA-15 surfaces with 4-aminophenylmercuric acetate (APMA) groups. As a result, an enzyme molecule (yeast cyt c) with a cysteine residue (cys-102) demonstrated strong adsorption, which provided high cyt c loading amounts, highly catalytic activity, and high stability against hydrothermal processes and organic solvents. To compare the immobilization of cysteine-containing cyt c through metal affinity interactions and a traditional covalent bond (a disulfide bond), we modified the SBA-15 surfaces with 3-mercaptopropyl-trimethoxysilane (MPTS) for further production of a disulfide bond with the cysteine residue of cyt c. The cysteine residue of the cyt c can covalently link to thiol-modified SBA-15 through the formation of a disulfide bond. In addition, a non-specific coordination from the thiol groups of SBA-15 to the heme Fe(III) of cyt c may destroy the catalytic center and cause the leaching of Fe(III) ions. Our previous studies of the molecular model have shown that the immobilization of cyt c through the cysteine residue can provide a correct orientation of the catalytic center, where the active site can easily approach the substrate molecules. Therefore, we have developed rapid and highly efficient approaches to immobilize a cysteine-containing enzyme through APMA ligands, which can both protect the protein folding and control the orientation to optimize the stability and catalytic activity.

Introduction

Cytochrome c (cyt c), a heme protein in mitochondria, acts as an electron shuttle in living cells.¹ Regarding *in vitro* functionality, cyt c shows peroxidase activity, which can decompose hydrogen peroxide and catalyze the oxidation of various types of polycyclic aromatic hydrocarbon PAHs (a carcinogenic and mutagenic activity).² The excellent activity of native enzymes is usually obtained under milder conditions; however, they lose catalytic activity under extreme conditions. In many cases of industrial processes, extreme pH, organic solvent, and high temperature are required for accelerating to the products. Increasing the thermal stability of an enzyme has many advantages such as raising reaction rates, increasing substrate solubility, and high temperature sterilization to prevent microbial contamination.³ Various methods for modifying the biocatalyst by biochemical and molecular biology approaches have been developed to overcome the

stability issues, generating robust biocatalysts. For example, site-directed mutagenesis of Gly82:Thr102 variant in cyt c showed that catalytic activity was improved by ten-fold in comparison with the wild type.⁴

Conversely, chemical modification can provide a more convenient method for improving stability and catalytic activity. Various chemical methods for modifying the enzyme molecules were also employed to obtain more stable derivatives such as amphiphilic polymer conjugation and cross-linked enzyme assemblies.⁵ Vazquez-Duhalt *et al.* modified cyt c with poly-(ethylene glycol) (PEG) to show that the modified cyt c exhibits cage-like polymer protection; and thus a high activity under high temperature.⁶ Enhancement of the stability and activity of an enzyme molecule could be obtained by immobilization of fragile enzymes on a solid support. One can also modify the solid surfaces with applicably functional groups, which can increase enzyme stability through the protection of solid supports and optimization of solvation in their microenvironment.⁷

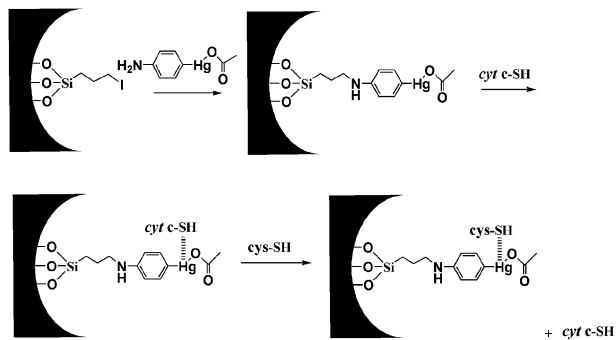
In recent years, mesoporous silica (MPS) has been widely applied in biotechnology.⁸ The uniqueness of large surface areas (near 1000 m² g⁻¹), highly ordered pore structure, and adjustable pore size (2–30 nm) extends MPS for applications in immobilizing enzymes⁹ or enzyme-mimicking compounds.¹⁰ Previously, we

^a Department of Life Science and Institute of Biotechnology, National Dong Hwa University, Hualien 974, Taiwan.
E-mail: chlee016@mail.ndhu.edu.tw; Fax: 886-3-863-3630

^b Department of Chemistry, National Taiwan University, Taipei, Taiwan 106

reported catalytic applications with an immobilized model compound (hydroxo-bridged di-nuclear phenanthroline cupric complex) in Al-MPS, which can mimic catechol oxidases.¹¹ Many research groups have also reported that the immobilization of enzymes on MPS exhibited improved enzyme stability, catalytic activity, products specificity, and resistance to extreme environmental conditions.¹² In our previous studies, we have immobilized cyt c in the nanochannels of MPS through electrostatic attractions and covalent bonding. The immobilized cyt c can increase both the catalytic activity and stability; therefore, an increase in the transformation of PAHs was observed.¹³ Thus, the nanochannels of MPS provide the confined spaces that could prevent cyt c from unfolding. Recently, we studied the orientation effect of cyt c within MPS through various covalent conjugations on the side groups of the cyt c molecule ($-\text{NH}_2$, $-\text{COOH}$, and $-\text{SH}$ site). The use of molecular modeling provided further insight into the relationship between the most efficient peroxidase activities and the orientation of the active site in a favorable location. The results indicated that the immobilization of cyt c in their cysteine residue has the highest activity because the active site of cyt c is pointed away from the silica wall, which would leave room for the substrate to diffuse into the nanochannels and react with the active site of cyt c in the nanospace of channels.¹⁴

The purpose of this work is mainly to develop a rapid and efficient method of cysteine-specific linking for immobilization of enzyme. We apply this method to linking cyt c into the nanochannels of MPS. Due to the high affinity of the mercury-sulfuric bonds, considerable research has reported that thiol groups can efficiently remove mercury ions for environmental purposes.¹⁵ The large surface areas of MPS can be modified with 3-mercaptopropyltrimethoxysilane (MPTS); thus a high loading of mercury(II) ions on the solid surfaces can be achieved. We then demonstrate that the mercury-modified SBA-15 can both efficiently immobilize cyt c through cysteine residue and provide a correct orientation for enhancing stability its peroxidase activity to catalyze the oxidation of polyaromatic hydrocarbon (PAH). The introduction of a metal affinity ligand in the nanochannels of SBA-15 to immobilize the cysteine-containing enzymes is a new approach, which can be applied to immobilize other type of enzyme molecules to optimize the orientation for biocatalytic applications (Scheme 1).¹⁶



Scheme 1 The representation of the synthesis of APMA-modified SBA-15 and the further immobilization of cyt c through metal affinity adsorption.

Experimental

Chemicals

Cytochrome c from *Saccharomyces cerevisia*, 3-aminopropyltrimethoxysilane (APTMS), glutaric anhydride (GAC), (3-Iodopropyl)trimethoxysilane, 4-aminophenylmercuric acetate (APMA), pyrene, Pluronic P123 ($\text{EO}_{20}\text{PO}_{70}\text{EO}_{20}$) were all obtained from Sigma Chemical Co. Hydrogen peroxide (35%), cetyltrimethylammonium bromide (CTAB), KCl, tetraethyl orthosilicate (TEOS), $\text{NaH}_2\text{PO}_4 \cdot \text{H}_2\text{O}$, and Na_2HPO_4 were all obtained from Acros.

Methods of preparation

(a) Synthesis of mesoporous silica. Highly ordered mesoporous structure of MCM-41 belongs to a family of mesoporous silicates (M41S) that was invented by Mobil researchers.^{17a} The MCM-41 material with pore diameters of 2.7 nm was prepared according to a method given previously.^{17b} Briefly, 27.4 g of (CTAB) was fully dissolved in 240 g of water. A portion of 35.6 g of sodium silicate solution was added to the above mixture under stirring. A sample of 42 g of 1.2 M H_2SO_4 was added slowly to the resulting mixture by pipette under stirring for 1 h at 32 °C and then hydrothermal at 100 °C for 2 days in a PTFE-lined autoclave. The final product was recovered by filtration, followed by washing twice with deionized water, dried at 100 °C, and calcined at 540 °C for 8 h.

In order to immobilize large APMA-cyt c complexes in the nanochannels of mesoporous silica, we choose large pore size of mesoporous silica (SBA-15) as the solid support. For the synthesis of SBA-15, poly(ethylene oxide)-*block*-poly(propylene oxide)-*block*-poly(ethylene oxide) triblock copolymer ($\text{EO}_{20}\text{PO}_{70}\text{EO}_{20}$, P123) was used as the structure-directing agent. By the addition of tetraethylorthosilicate (TEOS) under the acidic condition, the hydrolysis and co-condensation of silica source were produced the as-synthesized SBA-15. Briefly, SBA-15 was synthesized by dissolving 4.0 g of Pluronic P123 in 30 g of water and 120 g of 2 M HCl solution under stirring at 35 °C. Further, 8.5 g of TEOS was added into the above solution to further stir for 20 h. Then, the mixture was hydrothermal at 100 °C for overnight. The final product was recovered by filtration, followed by washing twice with deionized water, dried at RT, and calcined at 500 °C for 6 h.^{17c,d}

(b) Synthesis of mercapto-modified mesoporous silica. We also synthesized mercapto-modified mesoporous silica, which can immobilize cyt c through the formation of a disulfide bond. The synthetic condition was as follows. 0.5 g of calcined MCM-41/ or SBA-15 was placed in 100 ml of toluene and stirred for 30 min. A 2.5 g sample of mercaptotriethoxysilane (MPTS) was added to the resulting mixture. The reaction was allowed to proceed overnight at 100 °C. The solids were washed twice with acetone. The filtered sample was dried under vacuum.

(c) Synthesis of amine- and carboxylic acid-modified SBA-15. 0.5 g of calcined SBA-15 was well-dispersed in 100 mL of toluene, and 2.5 g of APTMS was added to the mixture. After stirring at room temperature for 1 h and refluxing at 100 °C for 20 h, the solids were centrifuged, washed by acetone, and dried in vacuum. The further derivation of carboxylic acid on the

surface of amine-modified SBA-15 was achieved by addition of amine-modified SBA-15 (1 g) in 30 mL of DMF and then 0.99 g of glutaric anhydride (GAC) was added. After stirring at room temperature for 1 h, the solution was heated to 60 °C with stirring for 9 h. The solids were washed twice with ethanol. The filtered sample was dried under vacuum.

The anchoring of APMA onto the surface of SBA-15 was accomplished by the following two approaches.

(d) Synthesis of SBA-15-APMA-1. The APMA-conjugated (3-iodopropyl)trimethoxysilane was synthesized by dissolving 0.5 g of APMA in 3 mL DMSO; 50 mL of THF was then added. Separately, 300 μL of (3-iodopropyl)trimethoxysilane was added to the above APMA solution and stirred at room temperature for 12 h; then the above APMA-silane-conjugated solution was added to 0.3 g SBA-15 while stirring at 90 °C for another 12 h. Samples were collected by centrifuge at 6000 rpm for 10 min, washed twice with DMSO and methanol, and further dried under a vacuum.

(e) Synthesis of SBA-15-APMA-2. 0.5 g of SBA-15 was placed in 100 mL toluene and stirred for 30 min. 1.0 mL of (3-iodopropyl)trimethoxysilane was then added to the resulting suspension and allowed to react for 20 h at 90 °C. Samples were washed twice with acetone. The filtered sample was dried under a vacuum. The conjugation of 4-aminophenylmercuric acetate (APMA) groups onto the iodine-modified SBA-15 was achieved through nucleophilic substitution of the SBA-15-iodine samples with the APMA. First, we dissolved 0.7 g of APMA in 10 mL DMSO; 25 mL of THF was then added. The APMA solution was further added to 0.3 g of iodine-modified SBA-15 while stirring at room temperature for 12 h. Samples were collected by centrifuging at 6000 rpm for 10 min, washed twice with DMSO and methanol, and dried under a vacuum (Scheme 1).

(f) Immobilization of cyt c. The immobilization of cyt c in different SBA-15 modifications was achieved according to the following procedure. First, a 20 μM cyt c stock solution was prepared by dissolving cyt c in a 0.05 M $\text{NaH}_2\text{PO}_4\text{--Na}_2\text{HPO}_4$ buffer solution (pH 7.4) while stirring. Then, 0.15 g of modified SBA-15 was added to 30 mL of the cyt c solution while stirring at 4 °C for 3 h. The SBA-cyt c solids were collected by filtration and dried under a vacuum. The cyt c loading was determined by monitoring the change of the strong absorption band at 407 nm.

(g) Stability of immobilized cyt c under KCl solution. Stability of cyt c in the KCl solution was determined by treating 0.05 g SBA-15-APMA-cyt c solids in 1 M KCl while stirring for 2 h, and then the samples were centrifuged. The leaching percentages of cyt c were determined by the Soret band absorption at 407 nm.

(h) Enzyme activity. It was reported that the cyt c/ H_2O_2 system could catalyze the oxidation of pyrene to form 1,8-pyrenodione and 9,10-anthraquinone.¹⁸ We performed a PAH assay to determine the enzymatic activity of various immobilized cyt c. Typically, 5 mg of SBA-15-APMA-cyt c solids were added to 5 mL of 20 μM PAHs solution (CH_3CN : 20% (v/v) and 0.05 M of $\text{NaH}_2\text{PO}_4\text{--Na}_2\text{HPO}_4$ buffer: 80%) at pH 6.1. After shaking the mixture for 1 min, 25 μL of 200 mM H_2O_2

was added. The mixture was shaken again at 250 rpm and 35 °C for 5 min. After the reaction was finished, the solids were separated from the reaction mixture by centrifuge. The reaction extent was determined by the intensity decrease of the absorption peaks at 335 nm (pyrene) in the solution phase. Specific activity was determined by measuring the number of moles of substrate oxidized by one mole of cyt c in 1 min and expressed as min^{-1} . The substrate adsorption on the solid supports was deducted from the measurement of a control blank experiment.

Characterization techniques

UV-Visible spectra were taken with a GeneQuant 1300 (GE Healthcare) spectrophotometer. The spectra were collected in the range of 200 to 800 nm wavelength against a standard. The surface area, pore size, and pore volume were determined by N_2 adsorption-desorption isotherms obtained at 77 K on a Micro-metric ASAP 2010 apparatus. The sample was outgassed at 10^{-3} Torr and 120 °C for approximately 3 h prior to the adsorption experiment. The pore size distribution curves were obtained from the analysis of the adsorption portion of the isotherms using the BJH (Barrett-Joyner-Halenda) method. The structures of mesoporous silica materials were analyzed by powder X-ray diffraction (XRD) with a Scintag X1 diffractometer using copper $\text{K}\alpha$ radiation at $\lambda = 0.154$ nm. A Bruker EMX EPR spectrometer (X-band) was employed to measure the electron paramagnetic resonance (EPR) spectra of the samples. We monitored the EPR spectra of the solid catalysts. The solid samples used for the analysis were introduced in a quartz tubing of 4 mm OD. The sample was degassed and sealed under a vacuum. The spectrometer was equipped with a variable temperature controller, allowing us to record spectra at low temperatures (above the boiling temperature of liquid helium). Typical spectrometer settings were: microwave frequency, 9.526 GHz; microwave power, 2 mW; center field, 2600 G; sweep width, 5000 G; time constant, 40.96 ms; and modulation amplitude, 5 G.

Results and discussion

Characterisations

(a) Adsorption studies. The nitrogen adsorption-desorption isotherms of these samples was shown in Fig. 1. We can observe that the surface area measured from nitrogen adsorption gradually decreased from 679 $\text{m}^2 \text{g}^{-1}$ for SBA-15 to 463 and 450 $\text{m}^2 \text{g}^{-1}$ for iodine- and thiol-modified SBA-15, and to 350 and 316 $\text{m}^2 \text{g}^{-1}$ for further modified APMA samples. At the same time, the pore size decreased from 7.4 nm for SBA-15 to 6.4 and 6.2 nm for SBA-15-I and SBA-15-SH, and to 5.3 and 5.4 nm for SBA-15-APMA-1 and -APMA-2. The decreases in surface areas and pore size indicate that the grafted groups were indeed attached on the inner wall surfaces of the nanochannels.

After the immobilization of cyt c (Fig. 1e and 1f), we noticed a great decrease for nitrogen adsorption (surface areas of the SBA-15-APMA-2-cyt c sample: 171 $\text{m}^2 \text{g}^{-1}$ and MCM-41-SH-cyt c: 136 $\text{m}^2 \text{g}^{-1}$) apparently because a good fraction of the surface areas of the channel was now occupied by the cyt c molecules. Although the pore size of MCM-41-SH (1.9 nm) is less than the molecular size of cyt c ($2.5 \times 2.5 \times 3.7$ nm),¹³ the

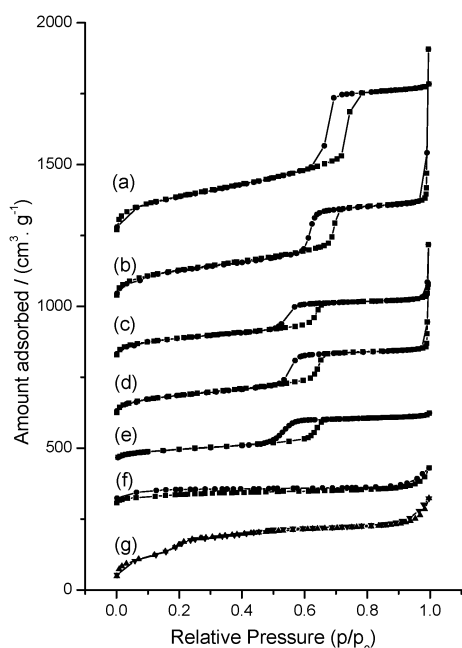


Fig. 1 Nitrogen adsorption–desorption isotherms of (a) SBA-15, (b) SBA-15-I, (c) SBA-15-APMA-1, (d) SBA-15-APMA-2, (e) SBA-15-APMA-2-cyt c, (f) MCM-41-SH-cyt c, and (g) after the calcination of the MCM-41-SH-cyt c sample at 560 °C for 8 h.

immobilization of cyt c apparently showed a drastic reduction in the surface areas. In addition, the MCM-41-SH samples also showed high loading amounts of cyt c molecules ($3.22 \mu\text{mol g}^{-1}$). In the immobilization process of the MCM-41-SH-cyt c sample, we also noticed that the cyt c changed the color from the bright red of the native cyt c form to the dark yellow of the immobilized form. This phenomenon may come from the unfolding 3-D structures and leaching heme groups of cyt c molecules, and thus the denatured cyt c molecules could easily enter the nanochannels of MCM-41-SH. We believe that the denatured form of cyt c molecules may be located both inside and outside the nanochannels of the MCM-41-SH. The nitrogen adsorption–desorption isotherms of the MCM41-SH-cyt c sample (Fig. 1f) showed the loss of the capillary condensation in the adsorption curve after the immobilization process. We inferred that large amounts of denatured cyt c molecules may occupy the nanochannels or clog the pores. To demonstrate that the structures of mesoporous silica were not destroyed during the immobilization process, we calcined the MCM-41-SH-cyt c sample in 560 °C for 8 h and further measured the nitrogen adsorption–desorption isotherms. We can observe that the elimination of organic molecules from the surfaces of mesoporous silica restored the surface areas ($667 \text{ m}^2 \text{ g}^{-1}$). Therefore, we confirm that the loss of the mesoporous adsorption curve may come from the cyt c molecules occupied the nanochannels or clogged the window of the pore.

Table 1 also shows the maximum adsorption of cyt c in various solid supports. The MCM-41-SH and SBA-15-SH samples can immobilize cyt c through a disulfide bond, which showed 3.22 and $2.27 \mu\text{mol g}^{-1}$ of maximum loading of cyt c, respectively. The SBA-15-APMA-2 sample provided a high affinity adsorption, which showed a little higher loading ($3.31 \mu\text{mol g}^{-1}$) of cyt c than the disulfide bond of SBA-15-SH-cyt c samples.

Table 1 Surface area, pore size, amount of cytochrome c adsorbed, and specific activity

Sample	Surface area ($\text{m}^2 \text{ g}^{-1}$)	Pore size (nm)	Max. loading of cyt c ($\mu\text{mol g}^{-1}$)	Specific activity (min^{-1})
SBA-15	679	7.4	N.D. ^a	N.D.
SBA-15-I	463	6.4	N.D.	N.D.
MCM-41	1015	2.7	N.D.	N.D.
MCM-41-SH	395	1.9	3.22	0.011
SBA-15-SH	450	6.2	2.27	0.004
SBA-15-APMA-1	350	5.3	3.15	0.773
SBA-15-APMA-2	316	5.4	3.31	0.841

^a N.D. = not determined.

(b) Powder X-ray diffraction (XRD). The XRD spectra of various solid mesoporous materials (Fig. 2), including SBA-15, SBA-15-I, SBA-15-APMA-1, and -APMA-2 samples give 2D hexagonal $P6mm$ pore structure showing (100), (110), and (200) diffraction peaks.¹⁹ The XRD diffraction intensity was slightly reduced after the modification of iodine and APMA on the surfaces of SBA-15. The XRD patterns showed that the modification of SBA-15 surfaces under organic solvents does not greatly affect the integrity of the well-defined mesostructure of solid supports. A slight decrease of the intensity in the SBA-15-APMA-2 sample may arise from the larger contrast in the density between the silica walls of the empty pores relative to that between the silica walls of the pores modified with APMA ligands.

(c) FT-IR spectra. We employed FT-IR spectroscopy to characterize the chemical bonds and surface organic groups in our SBA-15 samples (Fig. 3). The spectra of bare SBA-15 showed a broad band ($2700\text{--}3800 \text{ cm}^{-1}$) from the O–H stretch

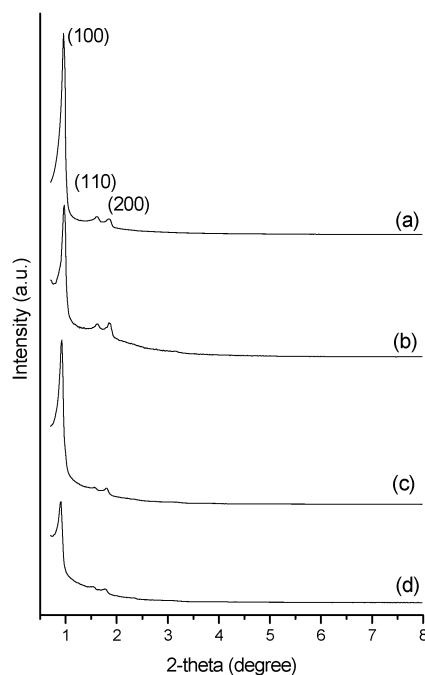


Fig. 2 XRD powder spectra of the following samples: (a) SBA-15, (b) SBA-15-I, (c) SBA-15-APMA-1, and (d) SBA-15-APMA-2.

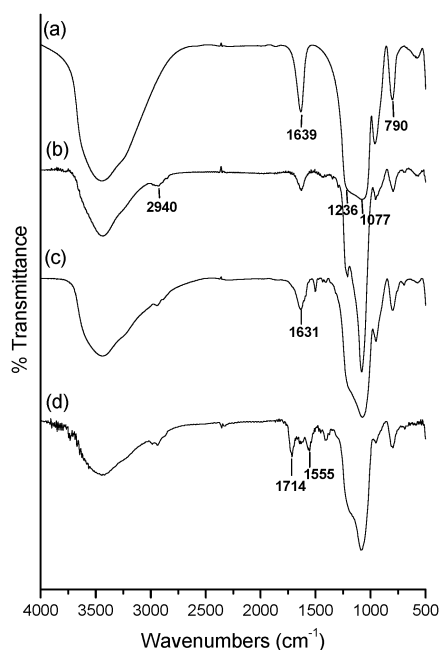


Fig. 3 FT-IR spectra of the following samples: (a) SBA-15, (b) SBA-15-I, (c) SBA-15-APMA-1, and (d) SBA-15-APMA-2.

of the absorbed molecular H_2O . The bands at 1077 cm^{-1} (with a shoulder at 1236 cm^{-1}) and 790 cm^{-1} are assigned to Si–O–Si vibration. The band at 1639 cm^{-1} is presumably caused by H_2O deformation (Fig. 3a). The (3-iodopropyl)trimethoxysilane-modified SBA-15 showed C–H stretches at 2940 cm^{-1} and 2980 cm^{-1} (Fig. 3b). The further conjugation of APMA molecules on the iodine-modified SBA-15 surfaces showed a C=O stretch mode (from the APMA molecule) at approximately 1714 cm^{-1} (Fig. 3d). Other peaks at 1555 are associated with the ring stretch absorption (the C=C stretch) of benzene.²⁰ We can observe that the peak intensity (from the contribution of APMA molecules) of SBA-15-APMA-2 sample (Fig. 3d) was higher than the SBA-15-APMA-1 sample (Fig. 3c). We can attribute the high intensity of the APMA signal to the high loading of APMA molecules in the nanochannels of SBA-15. The lower intensity of the vibrational signals of APMA molecules in the SBA-15-APMA-1 sample caused the overlap of the C=O stretch and H_2O deformation (1639 cm^{-1}); therefore, an asymmetry peak at 1631 cm^{-1} may come from the C=O stretch buried beneath.

(d) Diffuse reflectance UV-visible spectra. The low-spin Fe(III) center of the heme group in the native cyt c is coordinated to six ligands, four of which are nitrogen atoms of the heme group. The axial ligands are Met-80 and His-18. Fig. 4a shows the UV-Vis spectra of native cyt c.

The electronic absorption spectrum of native cyt c exhibits a Soret band absorption at λ_{max} 409 nm and a Q band at λ_{max} 529 nm. Another Q-band absorption at 555 nm only presents in low spin hemes of cyt c molecules (Fig. 4a). After cyt c immobilized in SBA-15-APMA-1 (Fig. 4b) and -2 (Fig. 4c) samples, the Soret band absorption at 409 nm was shifted to 407 nm. Previous studies indicated that the change of the heme iron sphere coordination through the weakening of the coordination of Met-80 to the heme iron and caused the shift

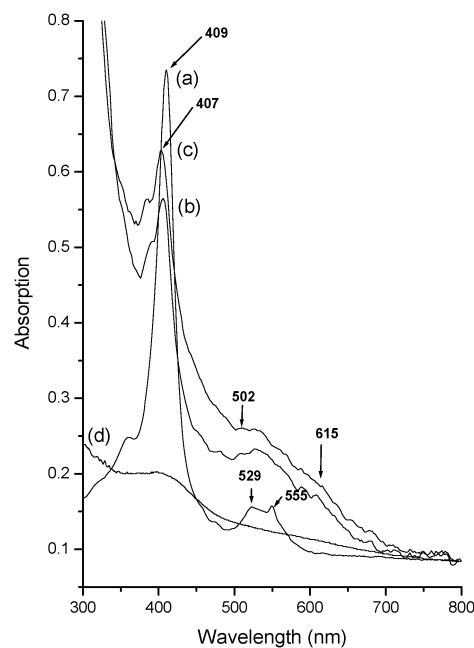


Fig. 4 (a) UV-Vis spectra of native cyt c in 0.05 M NaH_2PO_4 - Na_2HPO_4 buffer solution (pH 7.4). Diffuse reflectance UV-Vis spectra for the solid mixtures: (b) SBA-15-APMA-1-cyt c, (c) SBA-15-APMA-2-cyt c, and (d) SBA-15-SH-cyt c.

of the Soret band.^{21a} The alteration of low-spin configuration didn't produce a significant shift in the Q band at λ_{max} 529 nm; however. The disappearance of another Q-band absorption at 555 nm and the formation of a new Q band at 502 nm indicated that the low spin hemes of cyt c were converted to the high spin form (Fig. 4b and c).^{21b,c} Comparing the UV-Vis spectra of native cyt c and immobilized cyt c, we could verify that the cyt c altered the spin form after immobilization; however, it still retained the integrity through the immobilization in SBA-15-APMA supports (the retention of great Soret band intensity). Fig. 4d shows the spectrum of cyt c immobilized in SBA-15-SH through a disulfide bond. Although the SBA-15-APMA-cyt c and SBA-15-SH-cyt c samples have same cyt c loading ($2.0\text{ }\mu\text{mol}$ cyt c per g of supports), the Soret band intensity of the SBA-15-SH-cyt c sample at 407 nm is a greater decrease in intensity than that of the SBA-15-APMA-cyt c samples. The decrease in absorption intensity of the SBA-15-SH-cyt c samples may be due to an attack of the –SH group on the heme group, leading to the decomposition of cyt c and leach of the Fe(III) ions.

(e) Low temperature EPR studies. To study the stability of the heme Fe(III) center in SBA-15 supports, we performed EPR experiments at 10 K. The EPR spectrum of native low-spin-state cyt c with rhombic symmetry which was obtained in 2 M, pH 8.5 of *N*-(2-hydroxyethyl)piperazine-*N'*-(3-propanesulfonic acid) (EPPS) buffer showed spin at $g_1 = 3.1$ and $g_2 = 2.3$. In addition, a lower signal at $g = 4.3$ due to free Fe(III) ions may come from the deactivation of Heme-Fe(III) from the synthesis process (Fig. 5a).^{21a} Our previous studies have shown that the immobilization of cyt c in Al-MCM-41 through electrostatic attractions existed mostly in the high-spin Fe(III) state.¹³ High-spin Fe(III) is formed when Met-80 is replaced by H_2O during the immobilized process. Many studies have also reported that such

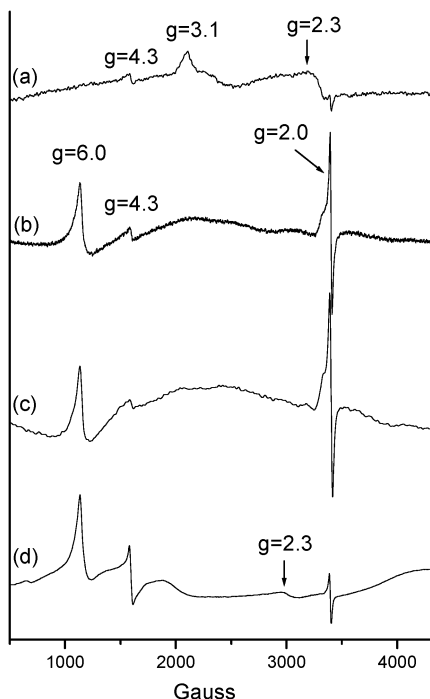


Fig. 5 EPR spectra at 10 K of cyt *c* (a) in 2 M EPPS buffer, pH 8.5, (b) immobilized on SBA-15-APMA-1-cyt *c*, (c) SBA-15-APMA-2-cyt *c*, and (d) SBA-15-SH-cyt *c*.

high spin species could increase both the activity and stability.²² When Met-80 was detached, the heme groove can fully open in the high spin configuration. Thus, the active center is easily accessible to the substrate and, therefore, an increase in the catalytic activity was observed. For our EPR spectra of SBA-15-APMA-1-cyt *c* and SBA-15-APMA-2-cyt *c* samples, we can observe the appearance of two signals at $g = 6.0$ and 2.0 , which is assigned to high-spin Fe(III). In addition, a lower intensity of the signal at $g = 4.3$ due to free Fe(III) ions which also appeared in the native cyt *c* sample (Fig. 5b and 5c). Fig. 5d shows the EPR spectrum of cyt *c* immobilized in the thiol-modified SBA-15 sample (SBA-15-SH-cyt *c*). We observed the following signals: $g = 6.0$ and 2.0 (assigned to high spin), $g = 2.3$ (low spin), and $g = 4.3$ (non-heme Fe(III)).²³ For the immobilization of cyt *c* through the formation of a disulfide bond, the thiol group of the SBA-15-SH sample may bind covalently to the heme iron, break down the heme structure, and ultimately free the Fe(III) ion, which will result in denaturation of the active site. Therefore, the high-spin Fe(III) is formed when Met-80 is replaced by H₂O; the low-spin configuration ($g = 2.3$) originates from the coordination of the thiol group (SBA-15-SH) to Fe(III).

Our EPR spectra indicated that the use of APMA as an affinity ligand to immobilize heme protein is a suitable approach, which can preserve the integrity of the heme structure of cyt *c*. However, the thiol-modified SBA-15 may poison the Fe(III) heme and leach the Fe(III) ions.

Binding affinity and catalytic activity of Cyt *c*

(a) Binding affinity in high concentration of KCl. We compared the strength for the binding affinity of cyt *c* in various SBA-15-modified surfaces (bare SBA-15, SBA-15-COOH,

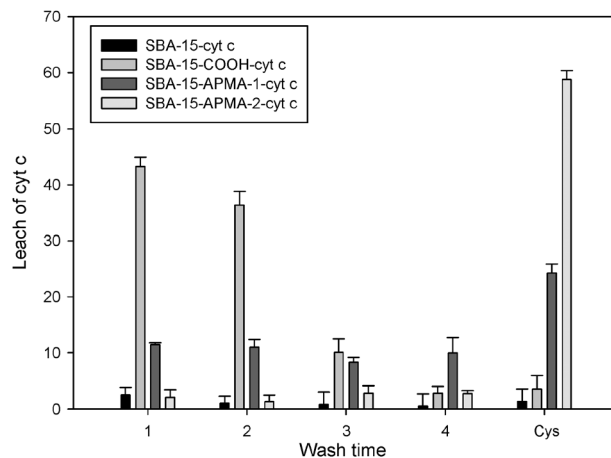


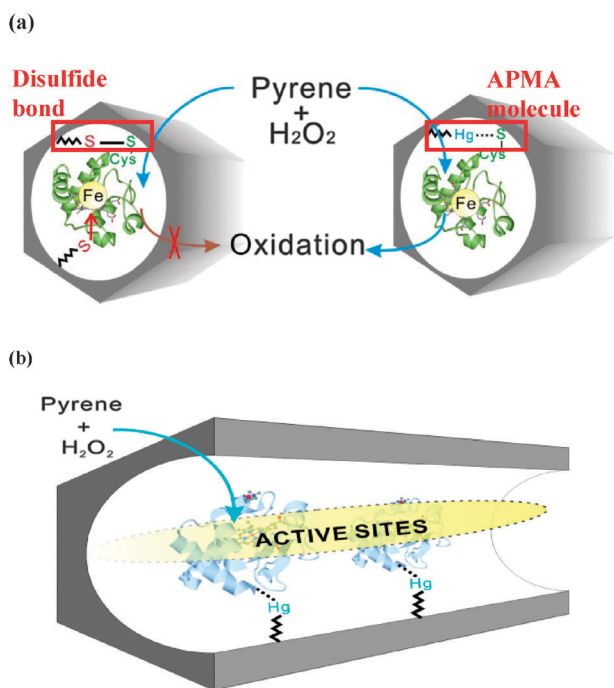
Fig. 6 Wash time 1–4: leaching amounts of cyt *c* after wash with 1 M KCl for 1–4 times. Cys: Replacement and release of mercury-adsorbed cyt *c* by adding L-cysteine.

SBA-15-APMA-1, and SBA-15-APMA-2). The isoelectric point (pI) of cyt *c* is 9.8, and therefore cyt *c* carries positive charges under neutral pH. For this reason, we chose the negative surfaces of bare SBA-15 and SBA-15-COOH to immobilize cyt *c* molecules. The pK_a value of the carboxylic acid and silanol group in the SBA-15 surface was 4.2 and 3.0, respectively.²⁴ Therefore, the bare SBA-15 surfaces showed higher percentages of negative charge than the SBA-15-COOH sample. We observed a very strong electrostatic attraction between the SBA-15 surfaces and the cyt *c* molecules; therefore, only 1–2% of cyt *c* leached from the bare SBA-15 surfaces after washing with 1 M KCl for 1–4 times (Fig. 6). On the other hand, the lower negative charged surfaces of carboxylic acid-modified SBA-15 showed higher leaching amounts of cyt *c* after washing with 1 M KCl for two cycles (1st: 43% and 2nd: 36%). By our new approach to immobilize cyt *c* through metal affinity interactions, the APMA molecules showed high efficiency to regulate the binding affinity between the SBA-15 surfaces and the cyt *c* molecules. The leaching amounts of cyt *c* from SBA-15-APMA-2-cyt *c* sample in 1 M KCl (1–4 cycles) were only 1.3–2.8%. However, SBA-15-APMA-1-cyt *c* sample showed higher leaching amounts of cyt *c* (8–11%) after 1–4 cycles. Due to the one step modification of SBA-15 surfaces with the APMA-propyltrimethoxysilane complexes of the SBA-15-APMA-1 sample, a high steric hindrance of APMA complexes leads to less modification in the internal surface of SBA-15. Thus, more cyt *c* were immobilized in the external surface of the solid supports; therefore, relatively high leaching amounts of cyt *c* were observed.

Furthermore, we added a 0.5 M L-cysteine solution to replace and elute the adsorbed cyt *c*. We observed that SBA-15-APMA-1-cyt *c* and SBA-15-APMA-2-cyt *c* samples could efficiently release the residual cyt *c* (24.3% and 58.8%, respectively) by L-cysteine through the exchange of adsorbed cyt *c* molecules. However, the cyt *c* release from SBA-15-cyt *c* and SBA-15-COOH-cyt *c* samples under L-cysteine solution was much less when compared with that of SBA-15-APMA-1-cyt *c* and SBA-15-APMA-2-cyt *c* samples. We could verify that the immobilization of cyt *c* was a metal affinity interaction through the mercury-adsorbed cyt *c*. By the development of this new strategy, we can reuse the solid supports

or enzyme molecules. Furthermore, we can apply to purify or separate the cysteine-containing enzymes through the size exclusion and metal affinity interactions.

(b) Catalytic activity. In the catalytic reaction of pyrene oxidation, we compared the catalytic activity of cyt c immobilized on MCM-14-SH and SBA-15-SH samples. Due to the small pore size of MCM-41-SH (1.9 nm), the native cyt c cannot easily enter the nanochannels of MCM-41-SH; therefore, the MCM-14-SH samples showed higher loadings of cyt c molecules in the external surfaces of mesoporous silica than the SBA-15-SH samples. Although the different ratio of cyt c existed in the external and internal surfaces of MCM-41-SH and SBA-15-SH samples, the specific activity of cyt c in the MCM-14-SH and SBA-15-SH samples all exhibited extremely low activity (0.011 and 0.004 min^{-1}). Therefore, we attribute the very low activity to the poison of catalytic ability of heme Fe(III) through the coordination of thiol groups (Scheme 2a). On the contrary, the immobilization of cyt c through metal affinity interactions of SBA-15-APMA-1 and -2 samples showed high activities (0.773 and 0.841 min^{-1}). Our previous molecular modeling studies have shown that the different conjugation approaches to immobilize cyt c can expose the catalytic active sites (Fe(III)-heme) in different environments. When cyt c is immobilized in the SBA-15-APMA-2 sample, there is only one mercapto group from cys-102 (cys-14 and cys-17 formed disulfide bonds to conjugate with the heme group), which would form Hg-S bonds with the SBA-15-APMA-2 sample. Since cys-102 is on the C-terminal helix, it can easily be attached to the pore surface of the SBA-15-APMA-2 samples. From the crystal



Scheme 2 (a) Immobilization of cyt c in the nanochannels of SBA-15 through a disulfide bond or a metal affinity interaction from the APMA molecule. (b) Orientation and specific binding of cyt c in SBA-15-APMA: active site (heme group) is pointed away from the silica wall and fully opened to the substrate (less steric hindrance).

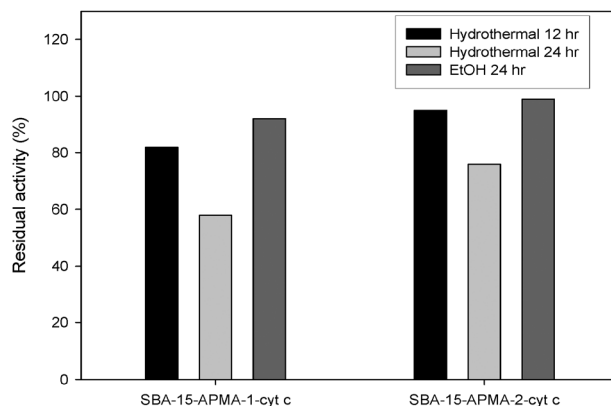


Fig. 7 Residual catalytic activity for pyrene oxidation of the SBA-15-APMA-1-cyt c and SBA-15-APMA-2-cyt c samples after hydrothermal for 12 h and 24 h, and EtOH treatment for 24 h.

structure of cyt c in an imaginary cubic box, we can observe that the active site of the Fe(III)-heme center is pointed away from the silica wall and fully accessible to the substrate.¹⁴ Therefore, the immobilization of cyt c in our new approach can leave room for the substrate to diffuse into the nanochannel and react with the active site of cyt c in the void space of channels (Scheme 2b).

(c) Hydrothermal stability. It has been hypothesized that the heme Fe(III) center breaks down irreversibly during hydrothermal heating at $100 \text{ }^\circ\text{C}$ and leaches out Fe(III) ions, which is evidenced by the irreversible decrease of Soret band absorption and loss of the catalytic activity. Fig. 7 shows the residual percentile catalytic activity of SBA-15-APMA-1-cyt c and SBA-15-APMA-2-cyt c samples after 12 and 24 h of hydrothermal treatment at $100 \text{ }^\circ\text{C}$ and the ethanol treatment at room temperature. The heat-treated SBA-15-APMA-1-cyt c sample retained 82% and 58% of residual activities after 12 and 24 h, respectively. The SBA-15-APMA-2-cyt c sample had high residual activity of 95% and 76% after 12 and 24 h, respectively. In addition, the two samples can retain most residual activity (92% and 99%) after the treatment of ethanol for 24 h. We can refer the high residual catalytic activity of the SBA-15-APMA-2-cyt c sample to the protection of cyt c from the strong affinity of APMA molecules and the confined space of SBA-15. Through this design, we can both increase the stability of the immobilized cyt c against extreme conditions and optimize the orientation to increase the reaction rate with the substrate molecules.

Conclusion

We demonstrate that the immobilization of cyt c in the nanochannels of SBA-15 through APMA molecules can provide both confined spaces and metal affinity interactions to stabilize the enzyme molecules against leaching under the high concentration KCl and hydrothermal processes. We summarize schematically the structural and bonding differences among cyt c immobilized in the nanochannels of SBA-15 through a disulfide bond and a metal affinity interaction from the APMA-modified SBA-15 in Scheme 2a. Our previous molecular modeling studies have shown that the peroxidase activity of

immobilized cyt c is related to the structural orientation of the cyt c in the SBA-15 nanochannels. The immobilization of cyt c through the cysteine residue leads the active site pointing away from the silica wall, which would leave room for the substrate to diffuse into the nanochannel and react with the active site of cyt c in the void space of channels (Scheme 2b). We therefore examined the two immobilized approaches through the cysteine residue of cyt c. While the cysteine residue can covalently link to thiol-modified SBA-15 through a disulfide bond; a non-specific coordination from the grafted thiol groups to the heme Fe(III) of cyt c can also destroy the catalytic center and cause the leaching of Fe(III) ions. The immobilization of cyt c through SBA-15-APMA showed that the confined space and metal affinity interactions from the APMA-modified SBA-15 indeed provided the stability toward the leaching of enzyme molecules under a high concentration of salts. In addition, the immobilization of cyt c through the APMA-modified SBA-15 can provide a robust catalytic center, where the active site can easily approach the substrate molecules. Thus, the SBA-15-APMA provided a correct orientation that could position the active site in a favorable location in the pores to facilitate its activity.

Acknowledgements

We wish to thank Prof. S. C. Ke of Department of Physics, National Dong-Hwa University for assisting with the EPR measurements at low temperatures. This work was supported by a research grant from the National Science Council of Taiwan (NSC 99-2113-M-259-006-MY2).

References

- J. Berg, J. Tymoczko and L. Stryer, *Biochemistry*, W. H. Freeman and Company, New York, NY, 6th edn, 2007, p. 2.
- (a) K. Ryu, J. Kim, J. Heo and Y. Chae, *Biotechnol. Lett.*, 2002, **24**, 1535; (b) R. Radi, L. Thomson, H. Rubbo and E. Prodanov, *Arch. Biochem. Biophys.*, 1991, **288**, 112; (c) A. Fujita, H. Senzu, T. Kunitake and I. Hamachi, *Chem. Lett.*, 1994, 1219; (d) J. Deere, E. Magner, J. G. Wall and B. K. Hodnett, *Biotechnol. Prog.*, 2003, **19**, 1238; (e) E. Busi, B. D. Howes, R. Pogni, R. Basosi, R. Tinoco and R. Vazquez-Duhalt, *J. Mol. Catal. B: Enzym.*, 2000, **9**, 39; (f) R. Akasaka, T. Mashino and M. Hirobe, *J. Chem. Soc., Perkin Trans. 1*, 1994, **1**, 1817; (g) P. Laveille, A. Falcimaigne, F. Chamouleau, G. Renard, J. Drone, F. Fajula, S. Pulvin, D. Thomas, C. Bailly and A. Galarneau, *New J. Chem.*, 2010, **34**, 2153.
- C. C. Akoh, S. W. Chang, G. C. Lee and J. F. Shaw, *J. Agric. Food Chem.*, 2008, **22**, 10445.
- (a) R. Vazquez-Duhalt, *J. Mol. Catal. B: Enzym.*, 1999, **7**, 241; (b) E. Torres, J. V. Sandoval, F. I. Rosell, A. G. Mauk and R. Vazquez-Duhalt, *Enzyme Microb. Technol.*, 1995, **17**, 1014.
- (a) M. I. Kim, J. Kim, J. Lee, H. Jia, H. Bin Na, J. K. Youn, J. H. Kwak, A. Dohnalkova, J. W. Grate, P. Wang, T. Hyeon, H. G. Park and H. N. Chang, *Biotechnol. Bioeng.*, 2007, **96**, 210; (b) S. L. Gao, Y. J. Wang, X. Diao, G. S. Luo and Y. Y. Dai, *Bioresour. Technol.*, 2010, **101**, 3830.
- (a) H. Garcia-Arellano, B. Valderrama, G. Saab-Rincon and R. Vazquez-Duhalt, *Bioconjugate Chem.*, 2002, **13**, 1336; (b) R. Vazquez-Duhalt, *J. Mol. Catal. B: Enzym.*, 1999, **7**, 241.
- (a) J. Kim, J. W. Grate and P. Wang, *Chem. Eng. Sci.*, 2006, **61**, 1017; (b) C. H. Lee, T. S. Lin and C. Y. Mou, *Nano Today*, 2009, **4**, 165; (c) X. S. Zhao, X. Y. Bao, W. P. Guo and F. Y. Lee, *Mater. Today*, 2006, **9**, 32; (d) Y. Urabe, T. Shiomi, T. Itoh, A. Kawai, T. Tsunoda, F. Mizukami and K. Sakaguchi, *ChemBioChem*, 2007, **8**, 668; (e) T. Itoh, R. Ishii, S. Matsuura, S. Hamakawa, T. Hanaoka, T. Tsunoda, J. Mizuguchi and F. Mizukami, *Biochem. Eng. J.*, 2009, **44**, 167.
- (a) M. Vallet-Regi, F. Balas and D. Arcos, *Angew. Chem., Int. Ed.*, 2007, **46**, 7548; (b) J. L. Vivero-Escoto, I. I. Slowing, B. G. Trewyn and Victor S. Y. Lin, *Small*, 2010, **6**, 1952; (c) M. Manzano and M. Vallet-Regi, *J. Mater. Chem.*, 2010, **20**, 5593; (d) A. Vinu, M. Miyahara and K. Ariga, *J. Nanosci. Nanotechnol.*, 2006, **6**, 1510; (e) Y. Fukushima, T. Kajino and T. Itoh, *Curr. Nanosci.*, 2006, **2**, 211; (f) Z. H. Dai, H. C. Bao, X. D. Yang and H. X. Ju, *Biosens. Bioelectron.*, 2008, **23**, 1070.
- (a) K. Ariga, A. Vinu, J. P. Hill and T. Mori, *Coord. Chem. Rev.*, 2007, **251**, 2562; (b) M. Hartmann, *Chem. Mater.*, 2005, **17**, 4577; (c) J. Lee, H. Bin Na, B. C. Kim, J. H. Lee, B. Lee, J. H. Kwak, Y. Hwang, J. G. Park, M. B. Gu, J. Kim, J. Joo, C. H. Shin, J. W. Grate and T. Hyeon, *J. Mater. Chem.*, 2009, **19**, 7864; (d) L. Jie, F. Jie, C. Z. Yu, L. Y. Zhang, S. Y. Jiang, T. Bo and D. Y. Zhao, *Microporous Mesoporous Mater.*, 2004, **73**, 121; (e) A. Vinu, V. Murugesan, O. Tangermann and M. Hartmann, *Chem. Mater.*, 2004, **16**, 3056; (f) Y. J. Wang and F. Caruso, *Chem. Mater.*, 2005, **17**, 953.
- L. Frunz, R. Prins and G. D. Pirngruber, *Chem. Mater.*, 2007, **19**, 4357.
- (a) C. H. Lee, S. T. Wong, T. S. Lin and C. Y. Mou, *J. Phys. Chem. B*, 2005, **109**, 775; (b) C. H. Lee, H. C. Lin, T. S. Lin and C. Y. Mou, *J. Phys. Chem. C*, 2009, **113**, 16058.
- (a) C. H. Lei, Y. Shin, J. Liu and E. J. Ackerman, *Nano Lett.*, 2007, **7**, 1050; (b) J. Liu, C. M. Li, Q. H. Yang, J. Yang and C. Li, *Langmuir*, 2007, **23**, 7255; (c) C. H. Lei, T. A. Soares, Y. S. Shin, J. Liu and E. J. Ackerman, *Nanotechnology*, 2008, **19**, 125102; (d) Y. J. Lu, P. J. Li, Y. L. Guo, Y. Q. Wang and G. Z. Lu, *Prog. Chem.*, 2008, **20**, 1172; (e) S. Matsuura, R. Ishii, T. Itoh, T. Hanaoka, S. Hamakawa, T. Tsunoda and F. Mizukami, *Microporous Mesoporous Mater.*, 2010, **127**, 61; (f) C. Ispas, I. Sokolov and S. Andrescu, *Anal. Bioanal. Chem.*, 2009, **393**, 543; (g) I. Oda, M. Iwaki, D. Fujita, Y. Tsutsui, S. Ishizaka, M. Dewa, M. Nango, T. Kajino, Y. Fukushima and S. Itoh, *Langmuir*, 2010, **26**, 13399.
- C. H. Lee, J. Lang, C. W. Yen, P. C. Shih, T. S. Lin and C. Y. Mou, *J. Phys. Chem. B*, 2005, **109**, 12277.
- K. C. Kao, C. H. Lee, T. S. Lin and C. Y. Mou, *J. Mater. Chem.*, 2010, **20**, 4653.
- (a) H. M. Kao, L. P. Lee and A. Palani, *Anal. Chem.*, 2008, **80**, 3016; (b) C. Delacote, Fabrice O. M. Gaslain, B. Lebeau and A. Walcarius, *Talanta*, 2009, **79**, 877; (c) E. Levi, Y. Gofer, Y. Vestfried, E. Lancry and D. Aurbach, *Chem. Mater.*, 2002, **14**, 2757.
- (a) Y. F. Chang and D. F. Tai, *Tetrahedron: Asymmetry*, 2001, **12**, 177; (b) D. F. Tai, Y. F. Chang and T. W. Chiou, *J. Chin. Chem. Soc.*, 2002, **49**, 957.
- (a) D. Y. Zhao, Q. Huo, J. L. Feng, B. F. Chmelka and G. D. Stucky, *J. Am. Chem. Soc.*, 1998, **120**, 6024; (b) C. H. Lee, T. S. Lin and C. Y. Mou, *J. Phys. Chem. B*, 2003, **107**, 2543.
- E. Torres, J. V. Sandoval, F. I. Rosell, A. G. Mauk and R. Vazquez-Duhalt, *Enzyme Microb. Technol.*, 1995, **17**, 1014.
- J. S. Beck, J. C. Vartuli, W. J. Roth, M. E. Leonowicz, C. T. Kresge, K. D. Schmitt, C. T. W. Chu, D. H. Olson, E. W. Sheppard, S. B. McCullen, J. B. Higgins and J. L. Schlenker, *J. Am. Chem. Soc.*, 1992, **114**, 10834.
- D. L. Pavia, G. M. Lampman and G. S. Kriz, *Introduction to Spectroscopy*, 3rd edn, 2001.
- (a) S. Oellerich, H. Wackerbarth and P. Hildebrandt, *J. Phys. Chem. B*, 2002, **106**, 6566; (b) F. I. Rosell, J. C. Ferrer and A. G. Mauk, *J. Am. Chem. Soc.*, 1998, **120**, 11234.
- (a) J. Deere, E. Magner, J. G. Wall and B. K. Hodnett, *J. Phys. Chem. B*, 2002, **106**, 7340; (b) K. A. Carrado, S. M. Macha and D. M. Tiede, *Chem. Mater.*, 2004, **16**, 2559; (c) A. Vinu, C. Streb, V. Murugesan and M. Hartmann, *J. Phys. Chem. B*, 2003, **107**, 8297.
- (a) R. E. M. Diederix, M. Fittipaldi, J. A. R. Worrall, M. Huber, M. Ubbink and G. W. Canters, *Inorg. Chem.*, 2003, **42**, 7249; (b) C. H. Lee, C. Y. Mou, S. C. Ke and T. S. Lin, *Mol. Phys.*, 2006, **104**, 1635; (c) T. Much, V. Wagner, U. Bass, M. Leufgen, J. Geurts and L. W. Molenkamp, *Synth. Met.*, 2004, **146**, 317–320.
- (a) I. I. Slowing, B. G. Trewyn and V. S. Y. Lin, *J. Am. Chem. Soc.*, 2007, **129**, 8845; (b) J. M. Rosenholm, A. Duchanoy and M. Linden, *Chem. Mater.*, 2008, **20**, 1126.